




Thermal Lag Correction From a GLIDER Payload CTD for Poor Temperature Data

FUSHUO CHU,^{1,3} ZONGSHANG SI,^{1,2,4}  CHONGGUANG PANG,^{1,2,4} and JIANCHENG YU⁵

Abstract—This paper describes the thermal lag correction for Glider Payload Conductivity Temperature Depth Profiler data with a poor sampling rate. In particular, the thermal lag correction is more vulnerable to the influence of temperature data. According to variations in salinity with depth and the vertical downcast speed of the glider, salinity data are divided into five parts, and a method based on Morison et al. is proposed to determine the correction parameters. At 40–94 dbar and 140–280 dbar, the salinity difference is dominated by the temperature difference. At 94–140 dbar, the salinity difference is immune to the temperature difference and has a greater influence on the thermal lag-induced salinity error correction. After the sectional correction, the accuracy of the typical salinity interval is upgraded from 0.011 to 0.006 psu, which shows the effectiveness of this sectional method on correcting temperature difference.

Keywords: Glider, salinity correction, thermal lag, temperature difference.

1. Introduction

The autonomous underwater glider (hereafter ‘glider’) is a new observation sampling platform. Based on buoyancy control and adjustments in attitude, gliders can move vertically in the water column and produce forward motion (Rudnick et al. 2004). Their powered batteries allow for weeks to months of collection time for in situ measurements in oceans

worldwide. In the mid-1990s, three operational gliders supported by the Office of Naval Research (ONR) were developed: (1) the Slocum glider built by Webb Research Corporation (Webb et al. 2001), (2) the Seaglider manufactured at the University of Washington (Eriksen et al. 2001), and (3) the Spray glider built at the Scripps Institution of Oceanography (Sherman et al. 2001). These gliders have been used for hundreds of at-sea days during various missions to collect ocean profiles, e.g., the US West Coast, the Mediterranean Sea, the Kuroshio and the Gulf Stream Currents (Davis et al. 2012; Todd et al. 2009).

Temperature data were observed with a specific sensor, while the salinity data were determined by the measured conductivity and temperature using the state equations (UNESCO 1981). As with a conventional CTD, there is a mismatch between the conductivity and temperature sensor responses that has been reduced with improvements in temperature sensor thermistor accuracy and the development of conventional CTDs. In addition, another mismatch due to the thermal inertia of the conductivity sensor has gained attention in recent years. When a CTD moves from hot to cold water, it diffuses heat stored in the conductivity cells over time; water passing through the conductivity cells then gains heat and changes its conductivity, especially when crossing strong temperature gradients. This problem, referred to as the thermal lag effect, was examined by Lueck (1990) and a numerical model for thermal lag correction was proposed by Lueck and Picklo (1990). Morison et al. (1994) suggested an improved method based on a temperature–salinity (T–S) profile. Johnson et al. (2007) described sensor corrections for SBE-41 CTDs and showed the importance of an intermittent pumping strategy and coarse sampling interval in a thermal lag correction. Based on Morison et al. (1994), Mensah et al. (2007) revisited the

¹ Key Laboratory of Ocean Circulation and Waves, Institute of Oceanology, Chinese Academy of Sciences, Qingdao 266071, China. E-mail: sizongshang@qdio.ac.cn

² Laboratory for Ocean and Climate Dynamics, Qingdao National Laboratory for Marine Science and Technology, Qingdao 266237, China.

³ University of Chinese Academy of Sciences, Beijing 100049, China.

⁴ Center for Ocean Mega-Science, Chinese Academy of Science, Qingdao 266071, China.

⁵ Shenyang Institute of Automation Chinese Academy of Sciences, Shenyang 110016, China.

thermal mass inertia coefficient for a glider traveling across a sharp salinity gradient.

However, for glider payload with an unpumped CTD, performing a thermal lag correction can be more difficult. Based on Morison et al. (1994), thermal lag correction for variable glider speeds was proposed; the correction relies on finding four variables by minimizing an objective function that measures the area between downcast and upcast T–S curves (Garau et al. 2011). This method has been improved by using a median filter in the case of a sharp thermocline (Liu et al. 2015). When compared with an unpumped CTD where the flow inside the cells depends on the velocity of the platform, the development of a pumped CTD with a constant flow speed can reduce thermal lag effects significantly (Alvarez et al. 2013).

The Shenyang Institute of Automation Chinese Academy of Sciences undertook a glider project in 2003 and developed a Sea-Wing glider that has successfully collected large amounts of temperature and salinity data in the northern region of the South China Sea (Yu et al. 2011). The glider, containing a pumped Glider Payload CTD, can reach a depth of 1000 m with a nominal vertical speed of 0.2 m/s. To maintain power, a fast interval sampling rate (0.167 Hz) that was much lower than the continuous sampling rate (1 Hz) and the conventional CTD sampling rate (16–36 Hz) was adopted. The difference between the downcast temperature and the upcast temperature is more obvious in the Glider Payload CTD with this low sampling frequency (see Sect. 2A), and glider data processing and quality control need to be reappraised (Janzen and Creed 2011).

2. Morison Salinity Correction

2.1. Data

The salinity data are obtained from a Sea-Wing glider that crossed a weak eddy twice at the initial study site in the north part of the South China Sea (113.227°E, 17.103°N) from 3 July to 16 July 2016 (Fig. 1). The CTD profiles were recorded exclusively from the glider without any CTD reference, and the glider CTD profiles are corrected with a set of glider-

derived parameters. During this campaign, we excluded 8 profiles from our 89 statistics that did not reach a given depth or, for some reason, no data were available. For each profile, we used different pairs of coefficients α and β to minimize the downcast and upcast T–S separation during one dive period, and assumed that the compared profiles correspond to the same mass (Garau et al. 2011). Satellite altimeter sea level anomaly (SLA) data were downloaded from the Archiving, Validation, and Interpretation of Satellite Oceanographic Data (AVISO)/Centre National d'Études Spatiales (CNES) website. The SLA is referenced to a 20-year mean from 1996 to 2016, and the horizontal resolution of the gridded data is 0.25°. The altimeter data are used to derive surface geostrophic current anomalies and show the locations of the eddy where the glider surveyed. Altimeter data can provide essential information on ocean circulation and altimetry-derived currents were found to be more reliable than data assimilative models (Liu et al. 2014).

2.2. General Correction

To suppress the salinity spiking effect, a 7-point median filter was chosen to smooth the temperature and salinity profiles (Mensah et al. 2007; Liu et al. 2015). All profiles were corrected by a centered window, where the values were replaced by the median value of the window, and thus, the thermal lag effects were identified.

For the thermal lag correction, Lueck (1990) developed a correction for the error, C_T , which can be expressed as follows:

$$C_T(n) = -bC_T(n-1) + \gamma a[T(n) - T(n-1)], \quad (1)$$

where n is the sample index, T is the temperature and γ is the sensitivity of conductivity to temperature; the constants a and b are given by:

$$a = 4f_n\alpha\beta^{-1}(1 + 4f_n\beta^{-1})^{-1}, \quad (2)$$

$$b = 1 - 2a\alpha^{-1}. \quad (3)$$

where f_n is the Nyquist sampling frequency and C_T is added to the measured conductivity to obtain an estimate of the true conductivity. The amplitude of

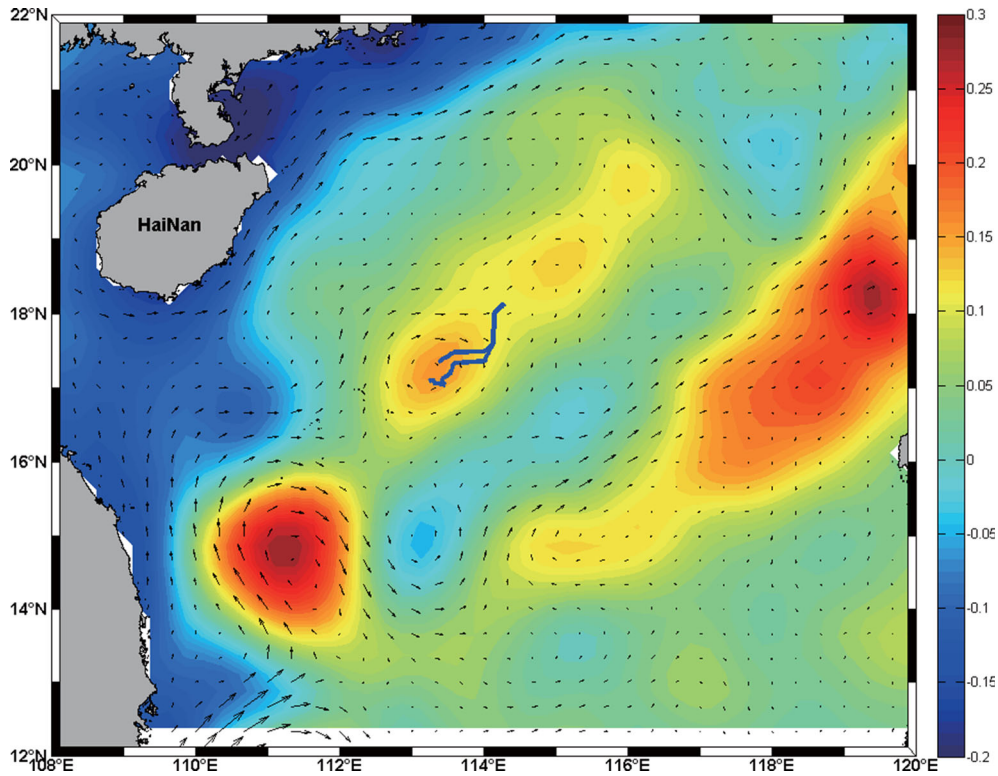


Figure 1

Sea level anomaly map (color scale) and associated geostrophic velocity anomalies on 3 July 2016. The blue line shows the glider track from 3 July to 16 July 2016

the error α and time constant τ ($1/\beta$) are given by the following rule formulas:

$$\alpha = 0.0135 + \frac{0.0264}{V}, \quad (4)$$

$$\tau = 7.1499 + \frac{2.7858}{\sqrt{V}}. \quad (5)$$

where V is the average flow rate through a conductivity cell.

Based on these formulas, Morison et al. (1994) tried to estimate the temperature inside the conductivity cell for the sole purpose of calculating salinity. This temperature version of (1) is given by:

$$T_T(n) = -bT_T(n-1) + a[T(n) - T(n-1)]. \quad (6)$$

Here, T_T is subtracted from the measured temperature to estimate the temperature in the conductivity cell that can be used for the salinity calculation. Thus, for Eq. (6), T_T does not rely on γ and has a faster calculation time.

A pair of profiles is selected to dismantle the thermal lag effect via the above method, which was provided during the second dive on July 15. After the median filter and general correction, the thermal lag effect at 50–140 dbar is overcorrected, while at 140–280 dbar, this correction can be neglected due to a significant temperature difference (Fig. 2c). An accurate estimate of salinity requires downcast and upcast temperature to be closely matched in space and time. However, the average temperature difference between the downcast and upcast temperatures is 0.41 °C, and the maximum difference can reach 1.12 °C, which is much larger than the allowable temperature difference (Fig. 2a). Thermal lag-induced salinity error need to be examined with such temperature difference which can also be found in other studies (Garau et al. 2011; Janzen and Creed 2011; Liu et al. 2015).

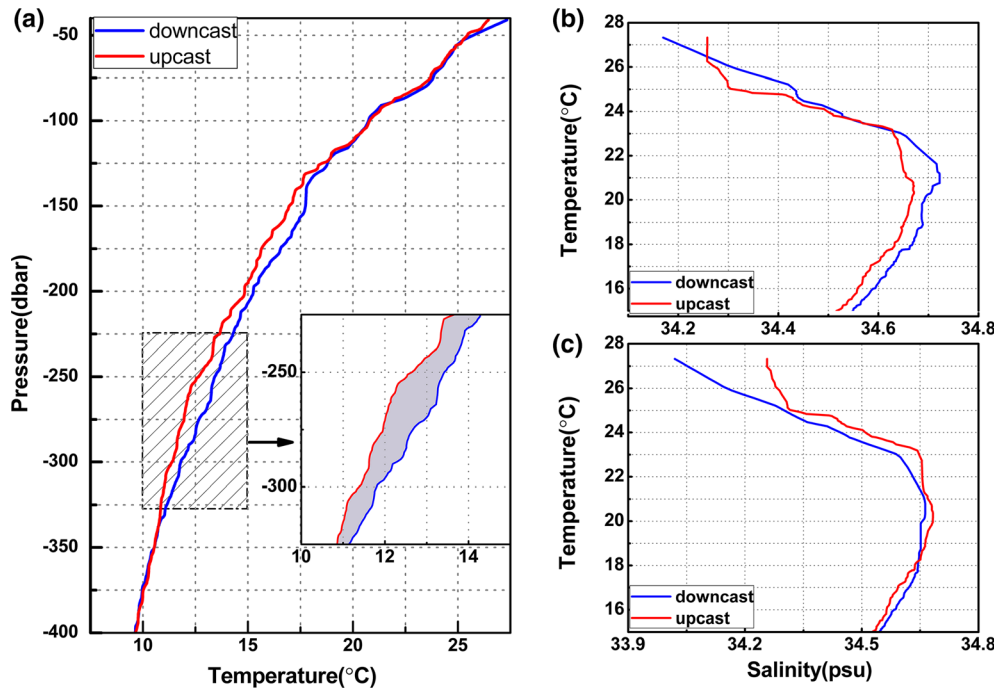


Figure 2

a Original temperature profile, **b** original salinity profile and **c** experimental salinity profile after alignment and a general thermal lag correction from the downcast (blue) and upcast (red)

3. Salinity Difference and Temperature Difference

3.1. AMSD and RMSD

For these 81 pairs of profiles, we interpolate the temperature and salinity data every 1 dbar and calculate the relative mean salinity difference (hereinafter referred to as ‘RMSD’) and the absolute mean salinity difference (hereinafter referred to as ‘AMSD’) at each pressure which are given by:

$$SD = S_d - S_u \quad (7)$$

$$RMSD = \sum_{i=1}^n \frac{1}{n} SD_i, \quad (8)$$

$$AMSD = \sum_{i=1}^n \frac{1}{n} |SD_i|, \quad (9)$$

where S_d and S_u represent downcast and upcast salinity, respectively. When temperature decreases with the depth, a slight positive salinity error occurs for the downcast period, and a slight negative salinity error occurs for the upcast period due to thermal lag effects; therefore, without other errors, SD will be

positive, and the value of AMSD is in accordance with RMSD. If SD is negative in some profiles, however, the AMSD will differ from RMSD and cannot be corrected for the thermal lag effect. This is shown in Fig. 3a. (Note that only 0–400 dbar data was used because similar to the case at 280–400 dbar, deeper than 400 dbar, the temperature and salinity have little changes and thermal lag effects are negligible. The following figures use the same data.). At 0–94 dbar and 140–280 dbar, the difference between AMSD and RMSD is large, which means the thermal lag correction is poor; at 94–140 dbar and 280–400 dbar, this difference can be negligible and suggests an influential thermal lag correction. To specify this difference between AMSD and RMSD and uncorrectable salinity data, we calculate the numbers and the averaged values of $SD < 0$ in each pressure value of the 81 profiles. To make the comparison more robust, we obtain the averaged values of SD in the form of absolute value (Fig. 4a). At 0–94 dbar and 140–280 dbar, there are more numbers of $SD < 0$, which are one-half and one-third of the

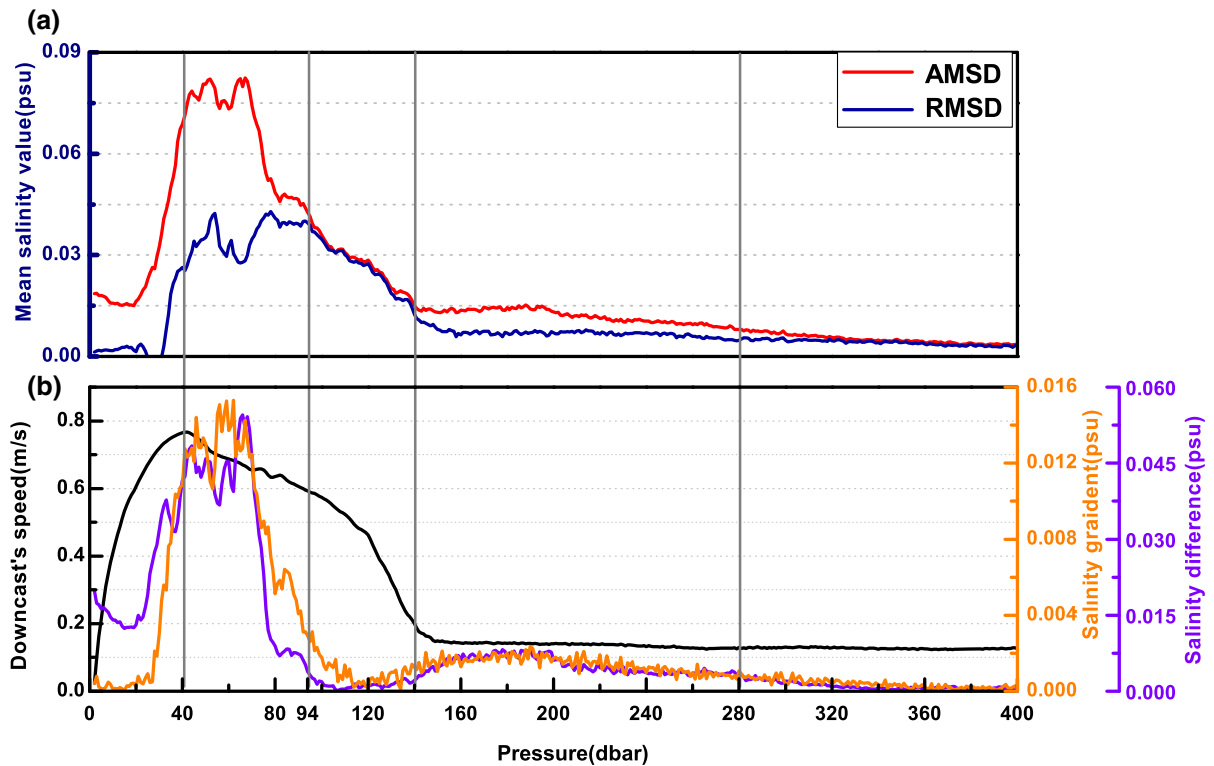


Figure 3

a Absolute mean salinity difference and relative mean salinity difference (red and blue, respectively). **b** The salinity difference between the downcast and upcast (violet) and salinity gradient (orange) with the glider's downcast vertical speed (black) averaged for 81 profiles; the solid gray line represents 40, 94, 140, and 280 dbar, respectively

whole profile, respectively, while the numbers at 94–140 dbar is inappreciable, with an average number of four. Similarly, the averaged values at 0–94 dbar and 140–280 dbar is greater than that at 94–140 dbar. Note that the numbers and the averaged values imply a poor salinity correction, mainly at 0–94 dbar and 140–280 dbar.

3.2. Pressure Profiles Division

A detailed sectional correction based on Morison et al. (1994) is applied in an unsatisfactory general thermal lag salinity correction, as previously mentioned. First, in a surface layer where the glider's vertical downcast speed increased to keep the pitch angle stable (Rudnick et al. 2018), the measurement resolution is low, and the blind zone depth interval can sometimes reach approximately 15 meters. Therefore, we divided this layer alone when the

glider's vertical downcast speed reached its maximum where the glider pitch angle is stable and has passed through the surface current layer where the correcting thermal mass effect based on interpolated salinity data has a large error. At depths below the surface, each profile is divided according to the difference between AMSD and RMSD. Depths where this difference is greater than 0.003 indicate an inconsistency between AMSD and RMSD, while depths where the difference is less than 0.003 indicate that AMSD and RMSD maintain a strong consistency. The average salinity gradient of the 81 profiles also serves as a criterion for the rationality of this division (Fig. 3b). This division is as follows: (I) At 0–40 dbar, the glider downcast vertical speed increases and reaches its maximum. (II) At 40–94 dbar, where the difference between AMSD and RMSD is greater than 0.003, salinity increases, and the salinity gradient maintains its maximum at 40–70

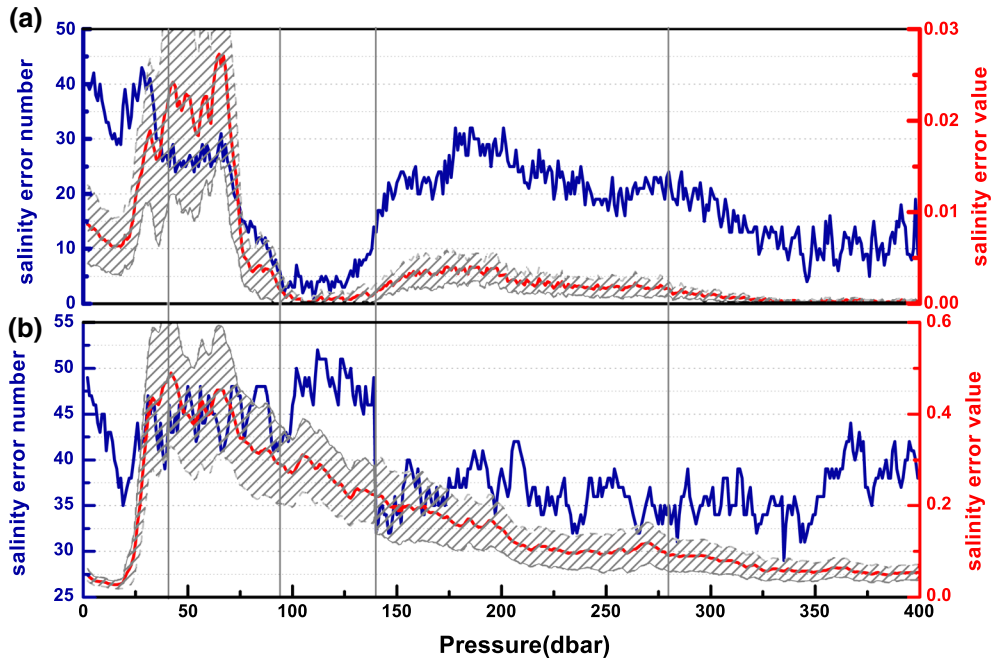


Figure 4

a The number of salinity error values (blue) calculated from summing the number of upcast salinity values larger than the downcast at each pressure. The average of salinity error values (red) derives from the salinity value of the error numbers between the downcast and upcast. **b** The number of temperature error values (blue) calculated from summing the number of downcast temperatures larger than the upcast in layer II and layer III, and upcast temperatures larger than the downcast in layer I, layer IV and 280–400 dbar. The average of salinity error values (red) derives from the temperature value of the error, while oblique lines represent the 95% confidence limits

dbar and then decreases rapidly. (III) At 94–140 dbar, where the difference between AMSD and RMSD is less than 0.003, the glider's vertical speed begins to decrease rapidly, and the salinity gradient changes very little. (IV) At 140–280 dbar where the difference between AMSD and RMSD is greater than 0.003, the glider's vertical speed remains stable while the salinity gradient changes rapidly. (V) At 280–1000 dbar, where the difference between AMSD and RMSD is less than 0.003, the thermal lag effects are negligible. Here, only (II)–(IV) were analyzed and corrected where the temperature difference and thermal lag effects were promising.

3.3. Consistency Between Salinity Difference and Temperature Difference

According to the state equations, the salinity is determined by conductivity and temperature. Ideally, the obtained temperature and salinity of the downcast

period correspond to those of the upcast; however, assuming the downcast temperature is inconsistent with the upcast temperature, the calculated downcast salinity will be different from the upcast salinity, so a further correlation analysis is carried out to check the consistency between the salinity difference and temperature difference (Longo et al. 2013). The relative mean temperature difference (RMTD) as follows:

$$TD = T_d - T_u, \quad (10)$$

$$RMTD = \sum_{i=1}^n \frac{1}{n} TD_i, \quad (11)$$

where T_d and T_u represent downcast and upcast temperature, respectively.

Figure 5 shows the correlation between RMSD and RMTD; data with a < 95% confidence level are abandoned (Di Federico et al. 2014). In layers II and III, significant negative correlations are found between RMSD and RMTD. However, in layer IV,

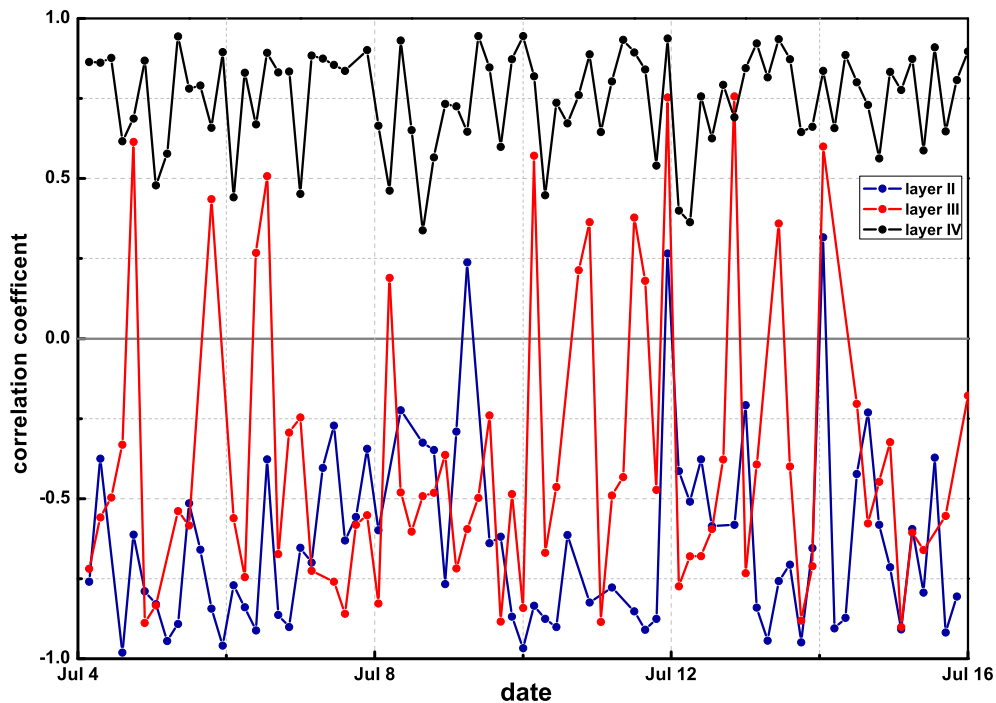


Figure 5

Correlation between the relative mean salinity error and relative mean temperature error in layer II (blue), layer III (red) and layer IV (black); data at the < 95% confidence level based on the t test have been abandoned

RMSD exhibits a high consistency with RMTD throughout all profiles with a significant positive correlation. This result shows that SD is related to TD, and this relationship varies with depth. When $SD < 0$ induced by TD, the thermal lag correction is unsatisfactory. Based on this dynamic, for layer II and layer III where there are significant negative correlations between TD and SD, we calculate the numbers and the averaged values of $TD > 0$ in each pressure value of the 81 profiles. For layer IV, where there is a significant positive correlation between the temperature difference and salinity difference, we calculate the numbers and the averaged values of $TD < 0$ in each pressure value of the 81 profiles. This result is elucidated in Fig. 4b. For layers II and IV, the calculated temperature numbers and the averaged values are large, which is consistent with Fig. 4a. For layer III, however, the calculated temperature numbers and average values has little effect on $SD < 0$. We will show that the thermal lag effect is more significant in the following analysis.

3.4. Correction Ratio and Temperature Difference

To examine the relationship between the thermal lag correction and temperature difference, we correct layers II, III and IV and define λ as the ratio of corrected RMSD to the uncorrected RMSD. Linear regression analysis between RMTD and η ($1/\lambda$) is shown in Fig. 6. In layer II (Fig. 6a), η is proportional to RMTD due to the negative correlation between TD and SD. When RMTD is positive, there are more numbers of upcast salinity greater than downcast salinity with a poor correction result. In layer IV (Fig. 6c), η is inversely proportional to RMTD. Similar to layer II, when RMTD is negative, the correction results are not ideal, and there is an overcorrection phenomenon in both layer II and layer IV ($\eta > 1$). However, in layer III (Fig. 6b), regardless of the RMTD value, the correction results are robust ($\eta < 0.4$). This shows that though RMTD and RMSD have a strong correlation in layer III (Fig. 5), the prominent thermal lag correction seems does not depend on the temperature difference.

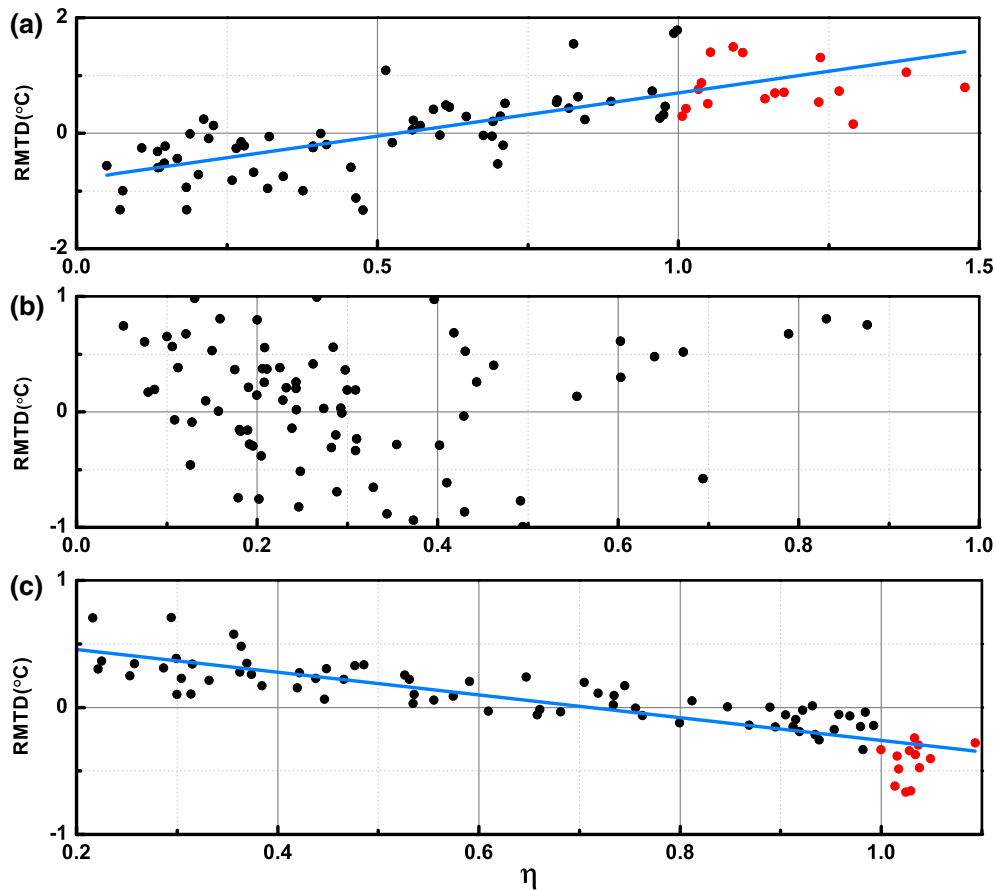


Figure 6

Regression analysis of correction ratio η and relative mean temperature difference (RMTD) in **a** layer II, **b** layer III and **c** layer IV. The red dots represent salinity overcorrection

3.5. Thermal Lag Correction Model Parameters

Generally, the temperature difference between the fluid within the conductivity cell and the water surrounding the thermistor is proportional to the temporal temperature gradient multiplied by $\alpha \times \tau$. Accordingly, we use $\alpha \times \tau$ as an indicator for the thermal lag correction (Fig. 7). In layer II and IV, the fitting result is unfavorable, which means the mean of the thermal lag correction is inconclusive. Furthermore, for layer III, the product of α and τ is consistent, and the mean value of $\alpha \times \tau$ is approximately 0.765 s, which is similar to the results of Eqs. (4) and (5) (when $V = 0.487$ m/s, the product of α and τ is approximately 0.755 s). This experiment indicates that the salinity difference and correction are dominated by the thermal lag effects in layer III.

4. Discussion

Our analysis clearly shows the correlation between the salinity difference and temperature difference. Indeed, electrical conductivity is a function of salinity, temperature and pressure and is mainly dominated by temperature signals. A slight temperature change can cause a conductivity change at same magnitude. This calculated salinity value from a wrong temperature and conductivity can be approximately regarded as a real measurement of the surrounding water mass, and thus, the effect of temperature difference on salinity can be neglected in this weak salinity gradient water column. However, the effect is significant in a sharp salinity gradient such as layer II and layer IV. Notably, this issue is

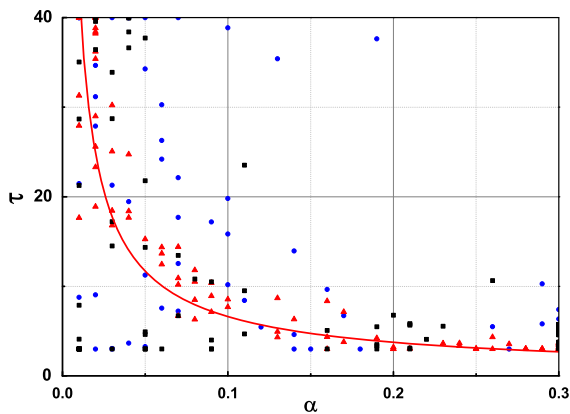


Figure 7

Values of conductivity cell thermal lag correction model parameters α and τ for 81 pair of profiles at layer II (blue dots), layer III (red triangles), and layer IV (black squares). The red solid line is the fitting curve of layer III; the fitting curves of layers II and IV are poor (not shown)

different from the short-term mismatch problem, which means different sensor response times between the temperature and conductivity cell; this is because for a sensor response mismatch the temperature and conductivity are not at the same pressure, while for the temperature difference, we obtain the same pressure. Therefore, we do not need to align temperature and conductivity sensor response times to eliminate this error because for a pumped CTD, this misalignment is negligible.

Thus, we have further examined the overcorrection of the sharp salinity gradient found in previous studies when temperature difference exist (Mensah et al. 2007). However, with respect to deploying a new pair of α and β coefficients for all profiles, a sectional correction is adopted. As discussed above, unlike conventional CTD casts from a surface vessel, a glider's vertical speed may vary through the water. Moreover, the glider's CTD sampling frequency is often lower than a high-resolution sampling of the CTD operated on a surface vessel, and the sampling interval may be uneven in space and time, particularly the long-term observation extent of the glider mission. Therefore, similar to SBE-41CP CTDs mounted on Argo profiling floats, we apply a different pair of coefficients to each profile to remove any salinity bias in a statistical sense (Johnson et al. 2007). The coefficients of each profile vary considerably, and when attempting to find a pair of

coefficients to correct the whole profile, the results are not ideal.

5. Correction

5.1. A Pair of Profile Corrections

A sectional correction is used to examine the overcorrection of layers II and III and the undercorrection of layer IV (Fig. 2c). After the sectional correction, the overcorrection is reduced dramatically compared to the general correction, though an unaltered correction exists at 40–60 dbar (Fig. 8a). In layer IV (Fig. 8b), the undercorrection for the salinity difference caused by the temperature difference is promising. The mean difference in salinity is reduced from 0.026 to 0.008, 0.037 to 0.009, and 0.030 to 0.018 in layer II, layer III and layer IV, respectively, and the average salinity separation between the original upcast and downcast profiles has decreased by a factor of almost 3. This indicates that the salinity difference induced by temperature difference has been significantly reduced, and thus, it can be used to improve the salinity correction for all profiles.

5.2. Comparing Sectional Corrections with Conventional Corrections

An ameliorated sectional method based on Morison et al. is applied in this experiment. According to our previous analysis, a conventional correction will lead to overcorrection (Fig. 2c). Another established glider salinity correction method was based on the relationship between α and β and the flow speed with unpumped CTD on board the Slocum gliders (Garau et al. 2011); the minimization of two CTD profiles is carried out using the optimization toolbox from MATLAB to find the minimum of a considered nonlinear multivariable function by means of a medium-scale optimization that uses sequential quadratic programming (SQP). Here, three salinity correction methods are used to examine the salinity correction result (Fig. 9); after the preliminary correction for the Morison method, the salinity inconsistency did not decrease at 140–280

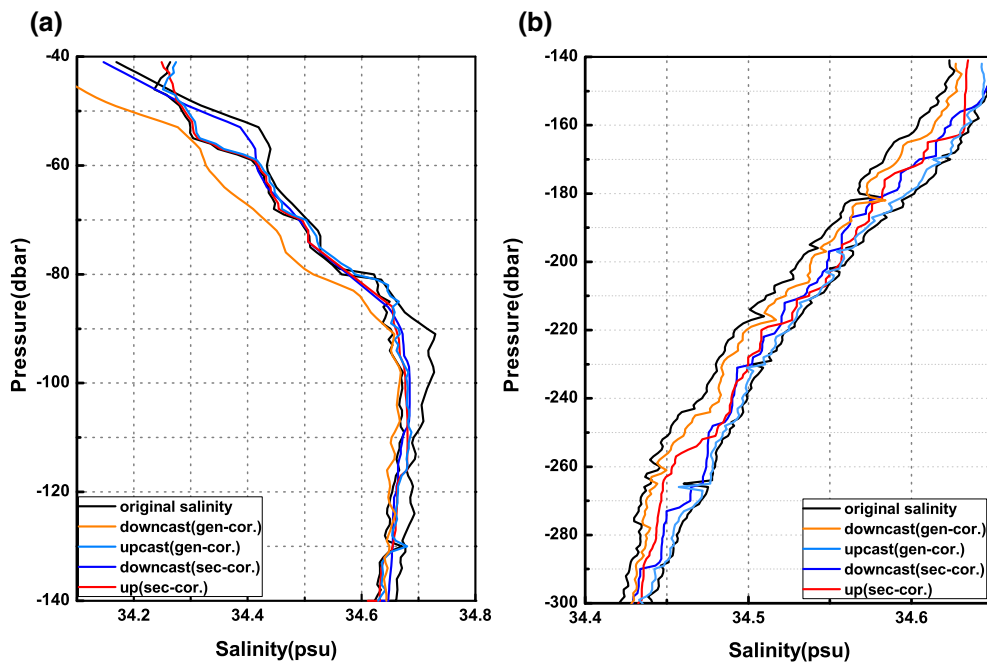


Figure 8

Sectional correction compared with original salinity at **a** 40–140 dbar and **b** 140–300 dbar. The black solid line is the calculated original salinity, the blue and red lines are downcast and upcast salinity corrected after sectional correction, respectively, and the orange and light blue lines are downcast and upcast salinity after general correction, respectively

dbar and was accompanied by an overcorrection at 40–140 dbar (Fig. 9b). Similarly, for the Garau method, the salinity correction did not produce the desired results, although the thermal lag salinity error was largely reduced compared to the original salinity data at 40–140 dbar (Fig. 9c). These preliminary experiments show that further improvements are needed for thermal lag corrections. When sectional Morison methods are used, there is a significant improvement both at 40–140 dbar and at 140–280 dbar with respect to the original Morison method and the Garau method (Fig. 9d). Thus, the sectional correction does not have an overcorrection or less-correction, which was expected in the case of temperature difference.

However, not all obtained salinity profiles need to be corrected by this sectional method. Temperature profiles and salinity profiles need to be examined carefully when a salinity correction is applied. Assuming the difference between the obtained downcast temperature and upcast temperature is larger than the allowable temperature range, a sectional

correction is necessary in the sharp salinity gradient. This specific method is to divide salinity profiles into a strong salinity gradient and a weak salinity gradient according to the difference between AMSD and RMSD (greater than 0.003 and less than 0.003, respectively) and the glider's downcast vertical speed (for example, we divide salinity profiles at 40–94 dbar and 140–280 dbar in this experiment) and apply the Morison salinity correction method, respectively. When the temperature difference is not obvious or the salinity varies little with depth, this correction method can be omitted. We wish to emphasize in this paper the influence of this difference on salinity corrections.

5.3. 81 Pairs of Profile Corrections

After the sectional correction is applied to 81 profiles, most mismatches are significantly reduced, especially in layer III, although such salinity differences are not easily seen from the 'contour' color dots generated by MATLAB (Fig. 10). In layer IV,

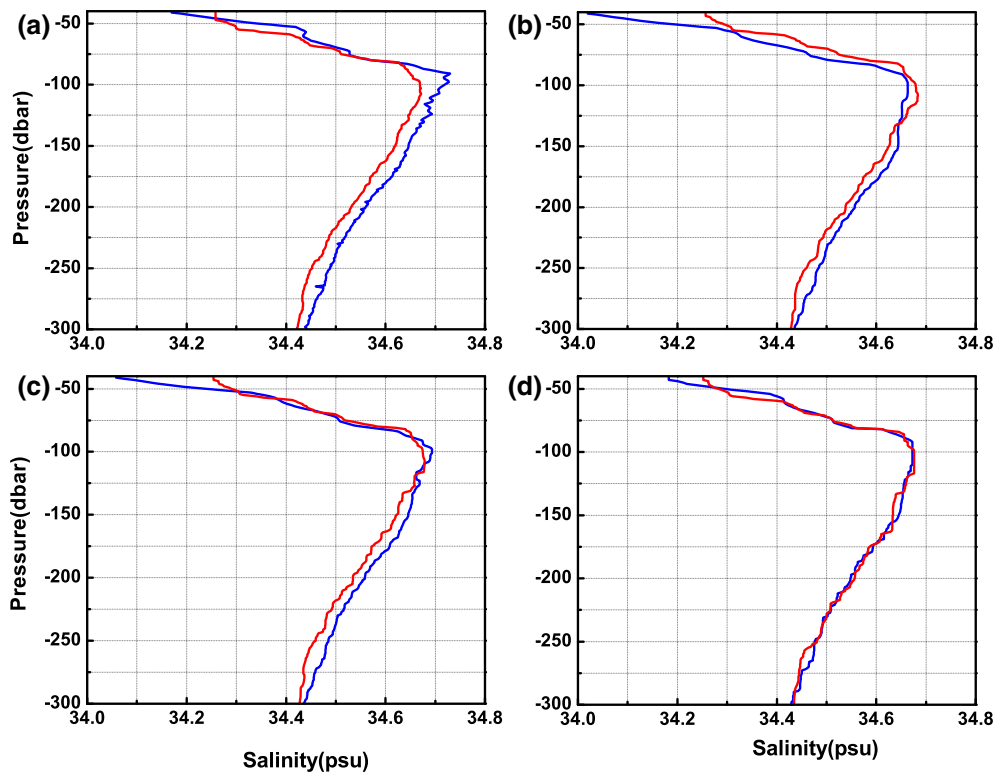


Figure 9

a Original salinity with corrected salinity using parameters from **b** Morison et al. (1994) and **c** Garau et al. (2011) and **d** sectional Morison method from the downcast (blue) and upcast (red)

several bands distorted due to the temperature data difference are smoother than the general correction. Through a quantitative comparison between the conventional Morison et al. correction and the sectional Morison correction using our 81 salinity profiles, the typical salinity correction ratio upgraded from 1.56 to 2.04, the salinity accuracy upgraded from 0.011 to 0.006 psu.

6. Summary and Conclusions

In this paper, the thermal lag correction of a glider with a pumped CTD is reevaluated. A thermal lag correction is powerful for small temperature difference data and a high sampling frequency (0.5 Hz); however, it is not ideal for large temperature difference data and a low sampling frequency (0.167 Hz), which has critical temperature (Fig. 2a). To examine the influence of temperature difference on the thermal

lag correction, we divide the data into five segments by variations in salinity with depth. In layer I (0–40 dbar), the glider's vertical downcast speed increased to keep the pitch angle stable; in layers II and III (40–94 dbar and 94–140 dbar, respectively) where the glider's vertical downcast speed is rapid, the correlation between SD and TD are negative, while in layer IV (140–280 dbar), the glider's speed is slow and the correlations are positive. In layer V (280–1000 dbar), the thermal lag effects and SD are negligible. To further show this correlation, we calculate the numbers and the averaged values of $SD < 0$ in each pressure of the 81 profiles. Similarly, we calculate the numbers and the averaged values of $TD > 0$ in layer II and layer III and the numbers and the averaged values of $TD < 0$ in layer IV. Figure 4 shows that in layer II and layer IV, both the numbers and the averaged values of SD are consistent with TD, and this anomaly is largest in layer II and is relatively small in layer IV. However, in layer III, the

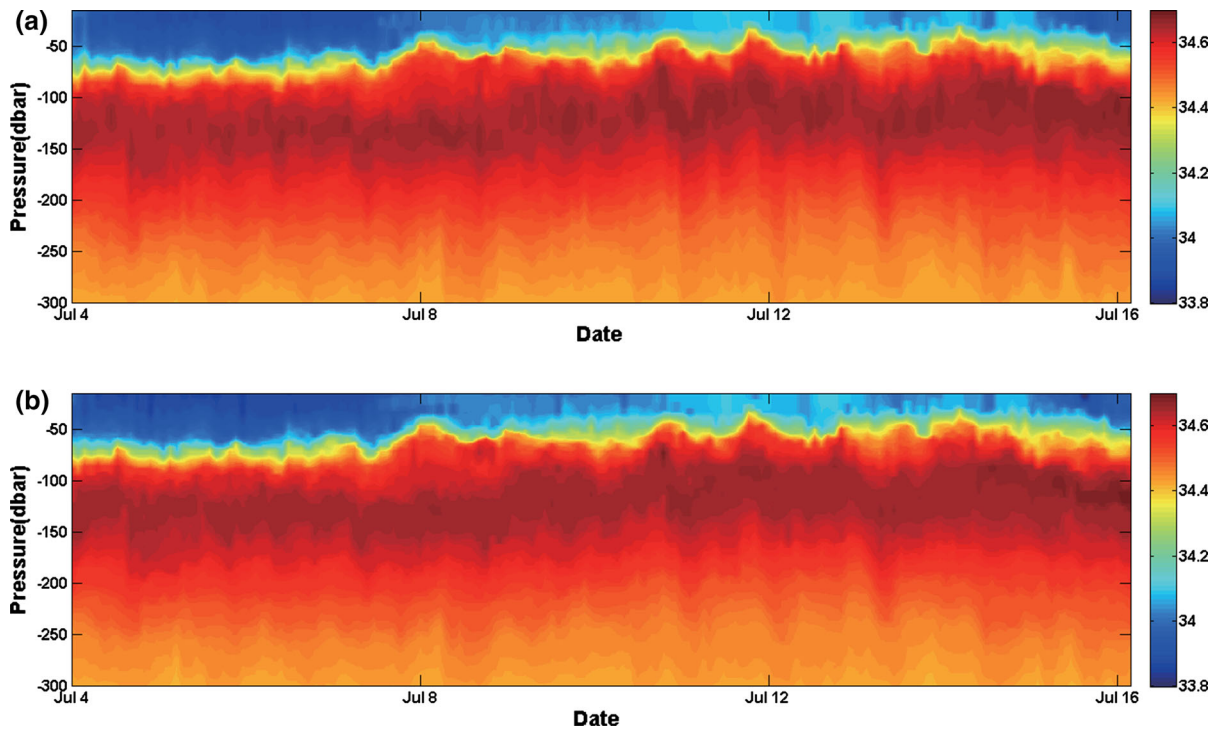


Figure 10

a General thermal lag salinity correction and **b** sectional thermal lag salinity correction

numbers and the averaged values of SD are insignificant compared to TD. Similarly, the correction ratio corresponds with TD in layers II and IV, but in layer III, regardless of RMTD value, the thermal lag correction is satisfied (Fig. 6). This may be because the temperature plays a leading role in the measurement of salinity with a negligible pressure effect. The incorrect measurement of temperature induced an incorrect conductivity, and thus, the obtained salinity is approximately equal to the salinity at a certain depth around. This inconsistency in salinity is clear in a sharp gradient, unlike in a weak salinity gradient, where the salinity values are almost the same at different depths, and the thermal lag effects are more important. Moreover, regression analysis reveals that in layer III, the thermal lag correction is consistent with the product of coefficients α and τ (Fig. 7). The suggested sectional correction here allows for an improvement in salinity accuracy with this different influence from the temperature. After applying this method in all profiles (Fig. 10), the typical salinity correction ratio is

upgraded from 1.56 to 2.04, and the salinity accuracy is upgraded from 0.011 to 0.006 psu, which shows the efficiency of this method.

As an important component of coastal ocean observing systems, gliders have been increasingly employed in oceans worldwide, and it is imperative to perform quality control on real-time data (Liu et al. 2015). Although a high-precision, stable pumped-CTD is being developed with reduced thermal lag effects (Schmitt and Petitt 2006), the influence of temperature error appearing in the thermistor is still not known. Thus, temperature data must be examined before using this improved sectional Morison thermal lag correction.

Acknowledgements

This work was supported by the Shenyang Institute of Automation, Chinese Academy of Sciences; we thank the crews for acquiring the numerous data used in this study. The authors would like to thank the National

Key R&D Program of China (2016YFC0301203) and National Natural Science Foundation of China (41576060) for their support in this research.

Publisher's Note Springer Nature remains neutral with regard to jurisdictional claims in published maps and institutional affiliations.

REFERENCES

- Alvarez, A., Stoner, R., & Maguer, A. (2013). Performance of pumped and un-pumped CTDs in an underwater glider. In *2013 Oceans - San Diego* (Oceans-Ieee).
- Davis, R. E., Kessler, W. S., & Sherman, J. T. (2012). Gliders Measure Western Boundary Current Transport from the South Pacific to the Equator. *Journal of Physical Oceanography*, 42(11), 05.
- Di Federico, V., Longo, S., Chiapponi, L., Archetti, R., & Ciriello, V. (2014). Radial gravity currents in vertically graded porous media: Theory and experiments for Newtonian and power-law fluids. *Advances in Water Resources*, 70, 65–76. <https://doi.org/10.1016/j.advwatres.2014.04.015>.
- Eriksen, C. C., Osse, T. J., Light, R. D., Wen, T., Lehman, T. W., Sabin, P. L., et al. (2001). Seaglider: A long-range autonomous underwater vehicle for oceanographic research. *IEEE Journal of Oceanic Engineering*, 26(4), 424–436.
- Garau, B., Ruiz, S., Zhang, W. G., Pascual, A., Heslop, E., Kerfoot, J., et al. (2011). Thermal lag correction on Slocum CTD glider data. *Journal of Atmospheric and Oceanic Technology*, 28(9), 1065–1071.
- Janzen, C.D., & Creed, E.L. (2011). Physical oceanographic data from Seaglider trials in stratified coastal waters using a new pumped payload CTD. In *OCEANS'11 MTS/IEEE KONA, 19-22 Sept. 2011*, pp. 1–7. <https://doi.org/10.23919/oceans.2011.6107290>.
- Johnson, G. C., Toole, J. M., & Larson, N. G. (2007). Sensor Corrections for Sea-Bird SBE-41CP and SBE-41 CTDs. *Journal of Atmospheric & Oceanic Technology*, 24(6), 1117–1130.
- Liu, Y., Weisberg, R. H., & Lembke, C. (2015). Chapter 17 - Glider Salinity Correction for Unpumped CTD Sensors across a Sharp Thermocline. In Y. Liu, H. Kerkering, & R. H. Weisberg (Eds.), *Coastal Ocean Observing Systems* (pp. 305–325). Boston: Academic Press.
- Liu, Y., Weisberg, R. H., Vignudelli, S., & Mitchum, G. T. (2014). Evaluation of altimetry-derived surface current products using Lagrangian drifter trajectories in the eastern Gulf of Mexico. *Journal of Geophysical Research: Oceans*, 119(5), 2827–2842. <https://doi.org/10.1002/2013jc009710>.
- Longo, S., Di Federico, V., Archetti, R., Chiapponi, L., Ciriello, V., & Ungarish, M. (2013). On the axisymmetric spreading of non-Newtonian power-law gravity currents of time-dependent volume: An experimental and theoretical investigation focused on the inference of rheological parameters. *Journal of Non-Newtonian Fluid Mechanics*, 201, 69–79. <https://doi.org/10.1016/j.jnnfm.2013.07.008>.
- Lueck, R. G. (1990). Thermal Inertia of Conductivity Cells: Theory. *Journal of Atmospheric & Oceanic Technology*, 7(5), 741–755.
- Lueck, R. G., & Picklo, J. J. (1990). Thermal Inertia of Conductivity Cells: Observations with a Sea-Bird Cell. *Journal of Atmospheric & Oceanic Technology*, 7(5), 756–768.
- Mensah, V., Menn, M. L., & Morel, Y. (2007). Thermal Mass Correction for the Evaluation of Salinity. *Journal of Atmospheric & Oceanic Technology*, 26(3), 665.
- Morison, J., Andersen, R., Larson, N., D'Asaro, E., & Boyd, T. (1994). The Correction for Thermal-Lag Effects in Sea-Bird CTD Data. *Journal of Atmospheric & Oceanic Technology*, 11(11), 1151–1164. [https://doi.org/10.1175/1520-0426\(1994\)011%3c1151:TCFTLE%3e2.0.CO;2](https://doi.org/10.1175/1520-0426(1994)011%3c1151:TCFTLE%3e2.0.CO;2).
- Rudnick, D. L., Davis, R. E., Eriksen, C. C., Fratantoni, D. M., & Perry, M. J. (2004). Underwater gliders for ocean research. *Marine Technology Society Journal*, 38(2), 73–84.
- Rudnick, D. L., Sherman, J. T., & Wu, A. P. (2018). Depth-Average Velocity from Spray Underwater Gliders. *Journal of Atmospheric and Oceanic Technology*, 35(8), 1665–1673. <https://doi.org/10.1175/jtech-d-17-0200.1>.
- Schmitt, R. W., & Pettit, R. A. (2006). A fast response, stable CTD for gliders and AUVs. In *Oceans*, (pp. 1–5).
- Sherman, J., Davis, R. E., Owens, W. B., & Valdes, J. (2001). The autonomous underwater glider “Spray”. *IEEE Journal of Oceanic Engineering*, 26(4), 437–446.
- Todd, R. E., Rudnick, D. L., & Davis, R. E. (2009). Monitoring the greater San Pedro Bay region using autonomous underwater gliders during fall of 2006. *Journal of Geophysical Research: Oceans*, 114(C6).
- UNESCO. (1981). Tent report of the Joint Panel on Oceanographic Tables and Standards. UNESCO Tech. Papers in Marine Science 36, 24 pp.
- Webb, D. C., Simonetti, P. J., & Jones, C. P. (2001). SLOCUM: An underwater glider propelled by environmental energy. *Journal of Ocean Engineering*, 26(4), 447–452.
- Yu, J.-C., Zhang, A. Q., Jin, W. M., Chen, Q., Tian, Y., & Liu, C. J. (2011). Development and experiments of the sea-wing underwater glider. *China Ocean Engineering*, 25(4), 721–736.

(Received July 28, 2019, revised October 28, 2019, accepted October 29, 2019, Published online November 11, 2019)